Available online at www.sciencedirect.com
SCIENCE DIRECT®
Solid State Sciences 5 (2003) 1009–1018
Solid State Sciences
www.elsevier.com/locate/ssscie

Cation ordering in $Li_2Mn_3MO_8$ spinels: structural and vibration spectroscopy studies

Pierre Strobel [a,*], Alejandro Ibarra-Palos [a], Michel Anne [a], Christiane Poinsignon [b], Alexandre Crisci [b]

[a] *Laboratoire de cristallographie CNRS, BP 166, 38042 Grenoble cedex 9, France*
[b] *LEPMI, ENSEEG, BP 75, 38402 Saint-Martin d'Hères cedex, France*

Received 24 March 2003; received in revised form 15 April 2003; accepted 22 April 2003

Abstract

Lithium-manganese oxide spinels with 1/4 manganese replaced by Mg, Ti, Co, Ni, Cu, Zn and Ga, yielding formula $LiMn_{1.5}M_{0.5}O_4$ (or $Li_2Mn_3MO_8$) have been prepared. Cationic ordering was known previously for M = Mg and Zn, resulting in a superstructure with primitive cubic symmetry. Given the poor chemical contrast of X-ray diffraction between Mn and Ti, Co, Ni, Cu or Ga, neutron diffraction studies were carried out. Evidence of cation ordering is found for M = Ni and Cu, but not for Ti, Co or Ga. These results are confirmed by FTIR and Raman spectroscopies. Doubly-substituted samples $(Li_{0.5}M_{0.5})[Mn_{1.5}M_{0.5}]O_4$ (overall formula $LiMn_3M_2O_8$) were also prepared for M = Mg and Zn. These do not form the primitive superstructure, a result ascribed to the lower manganese valence with respect to $LiMn_{1.5}M_{0.5}O_4$. Zn-containing spinels give rise to an extensive Li/Zn cation inversion, which also shows up as additional high-frequency bands in IR and Raman spectroscopies. This investigation shows that the cell volume is determined by the average octahedral-site cation radius, and that the main driving force for octahedral cation ordering is the charge difference between Mn and M atoms.

Keywords: Spinels; Cation ordering; Neutron diffraction; Infrared spectroscopy; Raman spectroscopy

1. Introduction

The mixed oxide $LiMn_2O_4$ is a normal spinel with space group $Fd3m$ (at room temperature), containing lithium on tetrahedral 8*a* sites and manganese on octahedral 16*d* sites. It is one of the major candidates for positive electrode materials in lithium batteries [1,2], due to its ability to insert or extract lithium with a theoretical capacity of 148 mAh/g on both lithium insertion and extraction. However, its practical use is hindered by capacity fading, especially at high temperature [3], due to (i) the presence of a cooperative Jahn–Teller distortion when the Mn^{3+} fraction exceeds 50%, (ii) structural instability in the high delithiation range. One of the main routes considered to reduce this fading is partial substitution of manganese by transition metals M, which has been thoroughly studied, especially for M = Cr, Co, Ni [4–6]. Such doping increases the manganese valence v(Mn) in the spinel phase, thus reducing the risk to reach the 50% Mn^{3+} fraction. But it also reduces the intrinsic capacity on lithium extraction, which is proportional to 4-v(Mn). On the other hand, the presence of M = Cr, Fe, Co, Ni or Cu gives rise to an extra plateau at high potential due to the oxidation of the dopant M and gives interest to compositions with relatively high substitution levels [7]. An especially interesting stoichiometry is $LiMn_{1.5}M_{0.5}O_4$ (or $Li_2Mn_3MO_8$), where the replacement of exactly 1/4 of the manganese yields tetravalent Mn only if M is divalent.

On the basis of available X-ray diffraction data, most electrochemical studies on such substituted materials assumed a random substitution of M on the manganese (16*d*) sites. However, the 3/4–1/4 ratio can favour an ordering of the 16*d* cations, as in the known compounds $Li_2Mn_3MgO_8$ [8] and $Li_2Mn_3ZnO_8$ [9]. In the latter case, the ordering was recently found to depend on preparation conditions [10]. Cation ordering has also been predicted from ab initio studies for most dopants [11,12]. For $Li_2Mn_3NiO_8$, conflicting results exist in the literature, with both unordered and ordered phases cited in ICSD [13–15]. Evidence of local ordering by infrared spectroscopy [16] and by MAS-NMR [17]

* Corresponding author.
E-mail address: strobel@grenoble.cnrs.fr (P. Strobel).

1293-2558/03/$ – see front matter
doi:10.1016/S1293-2558(03)00134-1

was reported earlier. In this work, we investigate a number of $LiMn_{1.5}M_{0.5}O_4$ compounds containing various M species with valences ranging from +2 to +4. Using neutron diffraction and vibration spectroscopies, we will show that compositions are indeed ordered for M = Ni and Cu, whereas the chemical contrast in X-ray diffraction is too weak to establish this by X- ray diffraction. The general trends of random vs. ordered 16d site occupation in $Li_2Mn_3MO_8$ spinels as a function of M charge and size will be discussed.

2. Experimental

Samples were prepared by solid state reaction using lithium carbonate, highly divided manganese dioxide and appropriate oxides or carbonates of substituting element (Mg, Ti, Co, Ni, Cu, Zn or Ga). Among possible trivalent substituents, aluminum was discarded because previous attempts showed synthesis difficulties: solid state reactions in the Li–Mn–Al–O system produce very stable $LiAlO_2$, which is practically impossible to eliminate once formed [18]. Mixtures were ground together and heated repeatedly at 750–900 °C in air with intermittent re-grinding and furnace cooling until the X-ray patterns did not change anymore. For compositions studied by neutron diffraction, quantities in the range 10–15 g were prepared. Details for the synthesis for M = Mg, Co, Ni and Cu have been reported previously [18,19].

Fired samples were analyzed by X-ray diffraction (XRD) using a Siemens D-5000 diffractometer equipped with a diffracted beam monochromator and operating with Cu $K\alpha$ radiation. Counting times higher than 20 s/step were systematically used to provide good statistics for Rietveld refinements. Neutron diffraction (ND) was carried out at Institut Laue-Langevin, Grenoble, France, using the powder diffractometers D2B ($\lambda = 1.5940$ Å) or D1B ($\lambda = 1.2806$ Å), on 10–15 g samples loosely packed in vanadium cylindrical cans.

Structural refinements were carried out using the Rietveld method with the WinplotR/Fullprof package [20]. Bond valence sums were calculated using the VaList program [21].

Infrared spectra were recorded on pellets prepared by diluting 1 mg sample in 150 mg TlBr; the powders were mixed and pressed under 8 tons/cm^2. The apparatus was a Nicolet 710 FTIR spectrometer used in transmission mode with a resolution of ± 2 cm^{-1}. The mirror velocity of the interferometer was reduced to 20 cycles/min to increase the beam intensity; 200 accumulations were carried out to record well resolved spectra.

For Raman spectroscopy, pellets of 10 mg sample dispersed in 200 mg KBr and carefully grinded before were pressed under 8 tons/cm^2. Spectra were recorded on a Jobin-Yvon T64000 spectrometer with typical acquisition time one hour.The radiation used was supplied by a Spectra Physics RM 20-18 laser operating at 514.5 nm with a 0.8 mW power.

3. Results

3.1. Composition and X-ray diffraction analysis

Table 1 summarizes the formulas of all samples, abbreviations used, and experimental studies carried out on each of them. $LiMn_{1.5}M_{0.5}O_4$ compositions were prepared with the following cation charge combinations: $Mn^{+3.33}/M^{+4}$ (M = Ti), $Mn^{+3.67}/M^{+3}$ (Ga, Co) and Mn^{+4}/M^{+2} (all other substituents). In the cobalt case, the charge distribution $Mn^{+3.67}/Co^{+3}$ (rather than Mn^{+4}/Co^{+2}) was established from magnetic susceptibility measurements [19]. Such a charge assignment has been confirmed by numerous studies on Mn–Co spinels [22–25]. Throughout this paper, $LiMn_{1.5}M_{0.5}O_4$ samples will be abbreviated according to the M element present, e.g. "Mg" for $LiMn_{1.5}Mg_{0.5}O_4$ (see Table 1).

Two compositions with double substitution were also prepared, with M replacing simultaneously 0.5 Mn and 0.5 Li. This corresponds to a $Li_{0.5}Mn_{1.5}MO_4$ overall formula (see Table 1, last two lines). Such compositions were prepared for substituents with weak octahedral preference in spinels, to avoid complex cation distributions in the resulting products [26,27], i.e. M = Mg and Zn (labeled "Mg-d"

Table 1
$AMn_{1.5}M_{0.5}O_4$ samples nominal composition, nomenclature and techniques used

Sample abbrev.	Formula	Nominal Mn valence	Diffraction data[a]	Spectroscopic studies	Ref.
Mn[a]	$LiMn_2O_4$	3.5	X, N	FTIR, Raman	(reference unsubstituted compound)
Ti	$LiMn_{1.5}Ti_{0.5}O_4$	3.33	X, N	–	this work
Ga	$LiMn_{1.5}Ga_{0.5}O_4$	3.67	X, N	FTIR, Raman	this work
Co	$LiMn_{1.5}Co_{0.5}O_4$	3.67	X, N	FTIR, Raman	this work
Ni	$LiMn_{1.5}Ni_{0.5}O_4$	4	X, N	FTIR, Raman	this work
Cu1,2[b]	$\approx LiMn_{1.5}Cu_{0.5}O_4$	4	X, N	–	this work
Mg	$LiMn_{1.5}Mg_{0.5}O_4$	4	X	(IR: see [16])	[8]
Zn	$LiMn_{1.5}Zn_{0.5}O_4$	4	X	–	[9,10]
Mg-d	$Li_{0.5}Mn_{1.5}MgO_4$	3.67	X	FTIR, Raman	this work
Zn-d	$Li_{0.5}Mn_{1.5}ZnO_4$	3.67	X	FTIR, Raman	this work

[a] X = X-ray diffraction; N = neutron diffraction.
[b] Cu1: purer, small-scale sample, Cu2: non-stoichiometric, larger sample used for neutron studies.

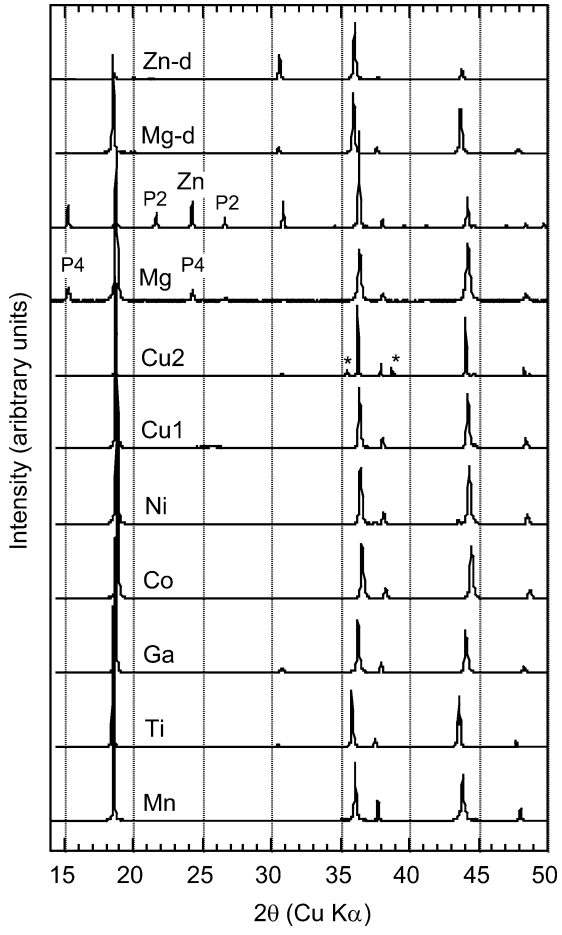

Fig. 1. XRD patterns in the $LiMn_{1.5}M_{0.5}O_4$ series (in same order as in Table 1, from bottom to top). P4: $P4_332$ cell reflections, P2: $P213$ reflections, * CuO impurity.

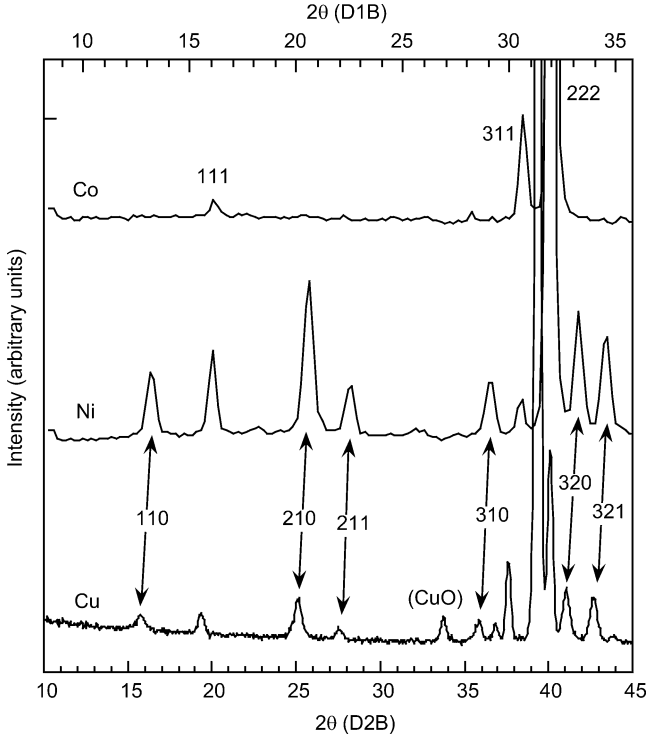

Fig. 2. Low-angle portion of neutron diffraction patterns of samples Co, Ni and Cu2. Arrows = primitive cubic cell reflections.

and "Zn-d", see Table 1, bottom). By modifying the charge on the Li (8*a*) site, this allows to vary the manganese valence v(Mn) while keeping the octahedral site contents ($Mn_{1.5}M_{0.5}$) unchanged.

Fig. 1 shows the XRD diagrams of samples prepared. Phase-pure compounds were obtained for all but the Ga and Ni samples, which contained very minor amounts of $LiGa_5O_8$ and NiO, respectively. For M = Cu, two samples were actually made: Cu1 (small batch) with negligible impurities, and Cu2 (large batch) containing a significant fraction of unreacted CuO; this could not be eliminated in the large quantity batch which had to be used for neutron diffraction. These impurities were taken into account in subsequent structure refinements by the Rietveld method.

Apart from impurities, significant differences can be seen throughout this series in Fig. 1. Firstly, the intensity of the 220 reflection (near 31 degrees 2θ) is strong for the Zn-containing samples, weak for Mg-d, and very weak but present for Cu, Ga and Ti. The intensity of this reflection is entirely due to the contribution of the 8a site scatterer, so that its presence reflects heavy atom occupation of the tetragonal 8*a* site. This is expected in Mg-d and Zn-d; in the other samples, it shows evidence of slight (Cu, Ga Ti) to strong (Zn) cation inversion between lithium and the M atom. Secondly, additional reflections are clearly present in the Mg and Zn samples—but, remarkably, not in Mg-d and Zn-d. They are all indexable in primitive cubic unit cells resulting from cation ordering, $P4_332$ for Mg and P_213 for Zn. Such extra reflections indicating cation ordering are not observed in the other samples.

3.2. Neutron diffraction and structural refinements

The differences in coherent neutron scattering lengths between manganese (−3.73 fm) and the neighbouring transition metal elements (Co: +2.50, Ni: +10.3, Cu: +7.72 fm) [28] allow to show experimentally whether or not these cations order on the octahedral sites. The results (see Fig. 2) clearly show the presence of superstructure reflections for M = Ni and Cu, and not for M = Co, Ga or Ti.

Structural refinements were carried out from powder diffraction data using pseudo-Voigt profiles. Final Rietveld refinements from neutron diffraction data included the following variables: (i) global parameters: zero-shift correction, 4 background polynomial coefficients, (ii) profile parameters for each phase detected: scale factor, unit cell parameters, profile parameters U, V, W and η, (iii) structural parameters (refined for the main spinel phase only): atomic positions, isotropic displacement parameters B_{iso}, cation occupancies on the 8*b* and 4*c* sites (the 12*d* site, occupied by the only small cation, namely Mn^{4+}, is not expected to give rise to mixed occupation). Because of expectable strong corre-

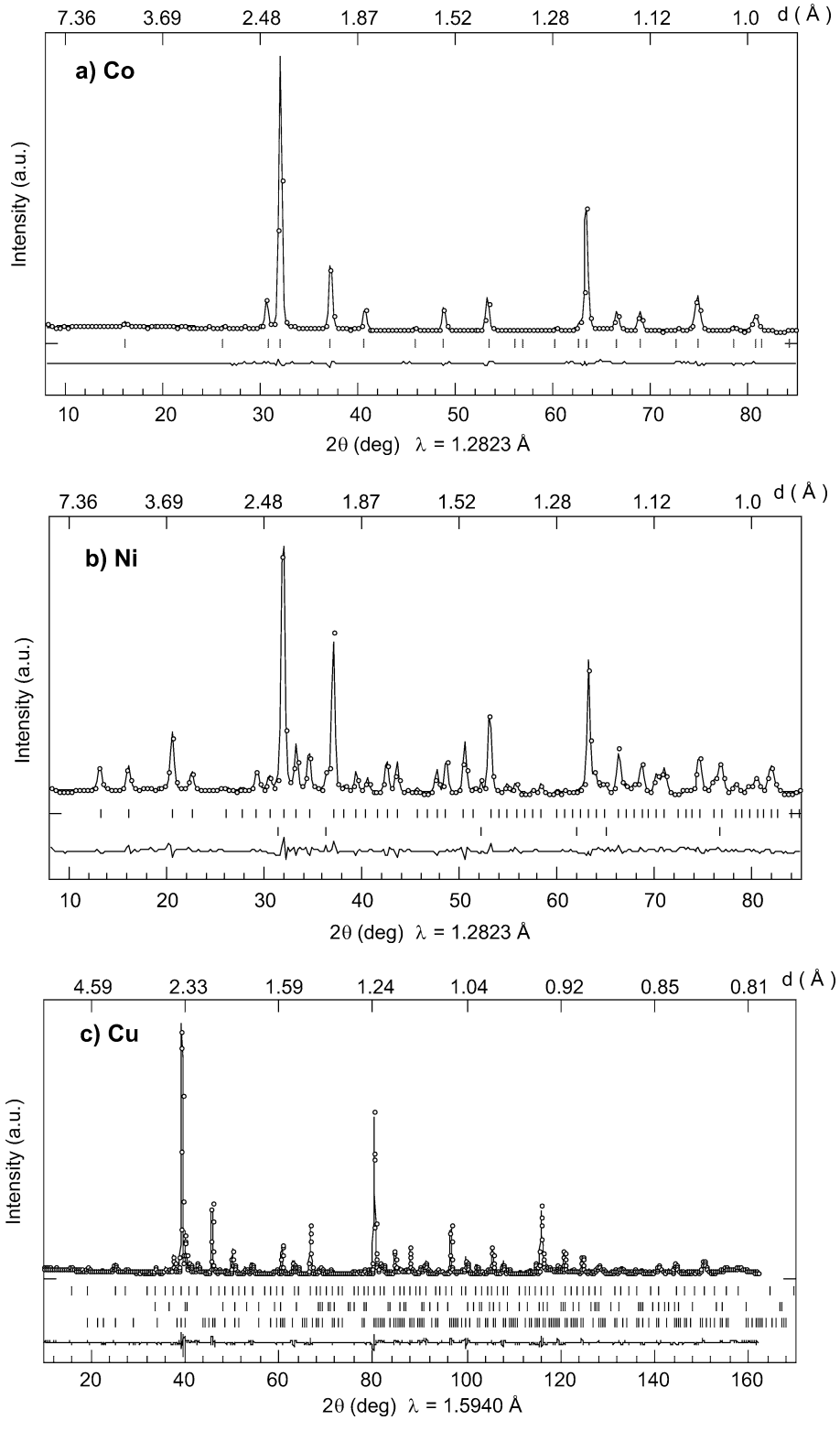

Fig. 3. Observed (points) and calculated (continuous line) neutron diffraction patterns of samples Co (a), Ni (b) and Cu2 (c). Differences $I_{obs} - I_{calc}$ are shown at the bottom.

lations, occupancies and B_{iso} parameters were refined separately, then B_{iso} of the atoms with variable occupation fixed in the final stages of refinements.This strategy resulted in 24 and 32 variables for samples Ni and Cu. Complete observed and calculated neutron diffraction patterns are given in Fig. 3.

Structural results are summarized in Tables 2 and 3, including Mg and Zn-containing samples, for which X-ray

data were used. The refinements confirmed the presence of a slight cation inversion for Ti (10%) and Ga (7%), while none was found for Co. The Ni and Cu phases clearly show an ordering of octahedral cations into 4*b* and 12*d* sites in space group $P4_332$. Both contain small (Ni) or large (Cu) fractions of lithium on the 4*b* site (see Table 3). In the latter case, the statistics were significantly improved by including also a fraction of Li_2MnO_3. Given the multiphase character of these two samples, no constrain on the total Ni or Cu content was used in the refinements. The under-stoichiometry in Cu and Ni found is consistent with the presence of unreacted NiO or CuO. Superstructure lines are weaker for Cu, due to (i) its smaller Fermi length difference with respect to Mn, (ii) partial Li/Cu inversion, which results in a ca. 50% lithium occupation of the octahedral Cu 4*b* site. Note that cation inversion has been observed previously in a number of Cu^{2+}-containing spinels, where it can be dependent on the sample annealing history [29].

Regarding the Mg and Zn phases, for which cation ordering was found previously [8–10], it is worth noting the difference in space group ($P4_332$ for Mg, $P2_13$ for Zn), which shows up in the X-ray diffraction pattern by the presence of additional reflections in the latter case (see Fig. 1). This symmetry difference is due to the strong tetrahedral preference of Zn^{2+}, which results in Li–Zn cation inversion, hence an additional 1:1 cation ordering on the tetrahedral sites which further lowers the symmetry. The structural formula of the Zn sample is then $(Li_{0.5}Zn_{0.5})[Mn_{1.5}Li_{0.5}]O_4$, and the octahedral site substituent is actually lithium. This inversion effect also occurs in the Zn-d sample, for which the Rietveld refinement gives the cation distribution $(Zn_{0.83}Li_{0.17})[Mn_{1.5}Li_{0.33}Zn_{0.17}]O_4$. Note that the two $Li_{0.5}Mn_{1.5}MO_4$ doubly-substituted samples differ considerably from the $LiMn_{1.5}M_{0.5}O_4$ Mg and Zn samples: they show no evidence of ordering, and have much larger cell dimensions than the corresponding $LiMn_{1.5}M_{0.5}O_4$ phases.

3.3. Infrared spectroscopy

Spinel-type compounds give rise to four T_{1u} infrared active modes [16,30]. As shown in Fig. 4a, the most intense of these in $LiMn_2O_4$ are two broad bands ν_1 and ν_2 at ca. 610 and 500 cm^{-1}, in agreement with the literature [31–33]. The third (ν_3) band is observed as weak shoulder on the low-energy side of the ν_2 one at 435 cm^{-1}. Figs. 4b and 4c show that these bands are practically unchanged for M = Ti, Ga and Co, confirming the absence of Mn/M cation ordering in these compounds.

For nickel substitution (Fig. 4d), FTIR shows a dramatic increase in the number of infrared active modes, in agreement with previous results [16]. This feature is readily explained by group theory analysis, which predicts an increase from 4 to 21 infrared active modes when the symmetry decreases from $Fd3m$ to $P4_332$ [34]. The Co–Ni comparison illustrates the power of vibration spectroscopy in determin-

Table 2
Summary of Rietveld refinements results on $AMn_{1.5}M_{0.5}O_4$ samples

Sample	A	M	Data used[a]	Global refinement parameters		Spinel phase results				Structural formula $(\ldots)_{tet}[\ldots]_{oct}$
				R_{wp}	χ^2	Space group	a (Å)	x(O)	R_{Bragg}	
Mn	Li	Mn	N	4.9	11.4	$Fd3m$ (297 K)	8.2449(2)	0.2632(3)	3.44	Li $[Mn_2]\,O_4 + 3\%\ Li_2MnO_3$[b]
Ti	Li	Ti	X	7.5	3.0	$Fd3m$	8.3039(2)	0.2626(2)	2.64	$(Li_{0.90}Ti_{0.10})\,[Mn_{1.50}Ti_{0.40}Li_{0.10}]\,O_4$
Ga	Li	Ga	X	13.7	4.5	$Fd3m$	8.2110(1)	0.2628(2)	2.30	$(Li_{0.93}Ga_{0.07})\,[Mn_{1.50}Ga_{0.43}Li_{0.07}]\,O_4 + 7\%\ LiGa_5O_8$[b]
Co	Li	Co	X	11.5	1.73	$Fd3m$	8.1379(2)	0.2629(2)	2.22	$Li\,[Mn_{1.50}Co_{0.50}]\,O_4$
Ni	Li	Ni	N	5.26	28.9	$P4_332$	8.1667(2)	c	5.17	$Li\,[Mn_{1.50}Ni_{0.44}Li_{0.06}]\,O_4 + 1.6\%\ NiO$[b]
Cu2	Li	Cu	N	8.7	7.5	$P4_332$	8.1888(2)	c	7.7	$(Li_{0.90}Cu_{0.10})\,[Mn_{1.50}Cu_{0.24}Li_{0.26}]\,O_4 + 6.2\%\ CuO, 6.2\%\ Li_2MnO_3$[b]
Mg	Li	Mg	X	15.4	1.37	$P4_332$	8.1869(4)	c	3.34	$Li\,[Mn_{1.50}Mg_{0.50}]\,O_4$
Zn	Li	Zn	X	9.88	0.89	$P2_13$	8.1824(2)	c	4.30	$(Zn_{0.50}Li_{0.50})\,[Mn_{1.50}Li_{0.50}]\,O_4$
Mg-d	$Li_{0.5}Mg_{0.5}$	Mg	X	10.1	2.7	$Fd3m$	8.2794(2)	0.2623(2)	2.68	$(Li_{0.50}Mg_{0.50})\,[Mn_{1.50}Mg_{0.50}]\,O_4$
Zn-d	$Li_{0.5}Zn_{0.5}$	Zn	X	6.13	1.39	$Fd3m$	8.2678(2)	0.2607(4)	2.05	$(Zn_{0.83}Li_{0.17})\,[Mn_{1.50}Li_{0.33}Zn_{0.17}]\,O_4$

[a] X = X-rays, N = neutrons (D2B for Mn and Cu, D1B for Ni—hence high χ^2 value).
[b] Mass fraction of foreign phase(s) from Rietveld refinement.
[c] Multiple sites—see details in Table 3 (Ni, Cu), Ref. [18] (Mg), Ref. [9] (Zn).

Table 3
Structure refinements results in $P4_332$ space group
(a) $LiMn_{1.5}Ni_{0.5}O_4$—neutrons (ILL-D1B, $\lambda = 1.282$ Å). 2-phase refinement: spinel 98.4%, NiO 1.6%

Atom	Position	x	y	z	B_{iso} (Å^2)	Occupation
Li	8*c*	0.007(2)	0.007(2)	0.007(2)	0.5 (fixed)	1 (fixed)
Mn	12*d*	1/8	0.380(1)	0.870(1)	0.71(13)	1 (fixed)
Ni/Li	4*b*	5/8	5/8	5/8	0.21(12)	0.87/0.13(2)
O1	8*c*	0.3844(6)	0.3844(6)	0.3844(6)	0.23(7)	1 (fixed)
O2	24*e*	0.1260(5)	0.1484(6)	0.8580(5)	0.23(7)	1 (fixed)

(b) $LiMn_{1.5}Cu_{0.5}O_4$—neutrons (ILL-D1B, $\lambda = 1.282$ Å). 3-phase refinement: spinel 87.8%, CuO 5.9%, Li_2MnO_3 6.3%

Atom	Position	x	y	z	B_{iso} (Å^2)	Occupation
Li/Cu	8*c*	0.003(2)	0.003(2)	0.003(2)	1.5 (fixed)	0.898/0.102(2)
Mn	12*d*	1/8	0.3829(6)	0.8671(6)	0.91(6)	1 (fixed)
Cu/Li	4*b*	5/8	5/8	5/8	1.0 (fixed)	0.46/0.54(1)
O1	8*c*	0.3863(3)	0.3863(3)	0.3863(3)	0.69(6)	1 (fixed)
O2	24*e*	0.1265(3)	0.1479(3)	0.8583(2)	1.13(4)	1 (fixed)

ing symmetry changes undetectable by X-ray diffraction (the Cu2 sample was not studied by IR spectroscopy due to its different stoichiometry and multiphase nature).

FTIR also gives valuable information on the Li–Mn–Mg–O and Li–Mn–Zn–O systems. In the former, the infrared spectrum of $LiMn_{1.5}Mg_{0.5}O_4$ was known to be fully consistent with cation ordering and cubic P symmetry [16]. We investigated here the Mg-d composition, for which no superstructure was detected in XRD in spite of a very similar composition and strong Mg–Mn chemical contrast. Its FTIR spectrum (Fig. 4e) indeed confirm the absence of additional vibration bands, meaning that an octahedral ($Mn_{1.5}Mg_{0.5}$) composition is not a sufficient condition to induce cation ordering. This point will be addressed in the discussion below.

In the Li–Mn–Zn–O series, the Zn-d composition gives rise to two additional IR peaks at 583 and 685 cm^{-1} (see Fig. 4f). These features can be attributed to the peculiar cation distribution revealed by XRD in this sample. The occurrence of extra infrared bands due to distribution changes involving cations with different masses has been reported previously; in particular, the high-frequency feature has been assigned to changes in tetrahedral site composition [35,36]. It is clearly visible at 680 cm^{-1} in the Zn-d sample, where the tetrahedral site is occupied mostly by the heaviest atom, here Zn (see Fig. 4f).

3.4. Raman spectroscopy

Raman spectra of samples Mn, Ga, Co, Ni and Zn-d are shown in Fig. 5. Normal spinels are characterized by a strong doublet at 590–630 cm^{-1}, with additional weaker bands at lower frequency. The five Raman-active modes expected for space group $Fd3m$ are listed in Table 4, together with experimental results. In a localised vibration analysis, the strongest A_{1g} band is viewed as the stretching of the 16*d*-site cation–oxygen bond [33,38]. For $LiMn_2O_4$, the rather large bandwidth of the main doublet can be ascribed to local lattice distortions resulting from the presence of mixed Mn^{3+}/Mn^{4+} valence on this site [38].

The Ga sample shows an almost unchanged spectrum (Fig. 5b), while in the cobalt case (Fig. 5c), the intensities of the T2g(3) and A1g bands are reversed, but without any additional band. The intensity reversal in the cobalt case can be due to (i) a significant difference in Raman scattering cross-section of the Co–O vibration, as in the case of chromium-doped $LiMn_2O_4$ [39], (ii) a small-polaron conductivity effect involving Co^{3+}/Mn^{3+}–Co^{2+}/Mn^{4+} couples; such an effect cannot take place in the gallium case.

As in the infrared spectrum, the Ni sample gives a very different spectrum with much sharper lines resulting from the symmetry lowering (Fig. 5d). The sharpness of the Raman bands can be seen as a signature of well separated, ordered Ni and Mn sites with integer valence distribution as in formula $(Li^{1+})_2(Mn^{4+})_3(Ni^{2+})O_8$. Note that in a recent Raman investigation of the $LiMn_{2-x}Ni_xO_4$ solid solution, a splitting of the main Raman doublet was also reported for $x = 0.5$, and for this composition only [40]; no structural explanation was proposed.

For the Zn-d sample, additional modes are also observed (Fig. 5e). The charge distribution is more complex in this case, with a significant fraction of heavy atom (Zn) occupying the tetrahedral 8a site (see Table 2, last line). This is the probable origin of the new feature at 700 cm^{-1}; similar high-frequency features have been observed on inverse spinels such as $V[LiNi]O_4$ [41]. The splitting of the main doublet, which resembles that observed for nickel substitution, shows that there is a local lattice distortion in the 16*d* sites, leading to a loss of translation invariance. Li^+ and Zn^{2+} actually have larger octahedral ionic radii than Ni^{2+} [42]. The absence of long-range cation ordering in Zn-d, contrary to the Ni sample, can be due to the fact that $LiMn_{1.5}Ni_{0.5}O_4$ and $Li_{0.5}Mn_{1.5}ZnO_4$ differ considerably not only in cation distribution, but also in manganese valence (+4 in Ni sample, +3.67 in Zn-d). This point will be addressed in the discussion below.

Finally, the frequencies of Mn–O vibrations depends on bond lengths and strengths, hence on the oxidation state of manganese. Table 4 shows a clear shift in Raman

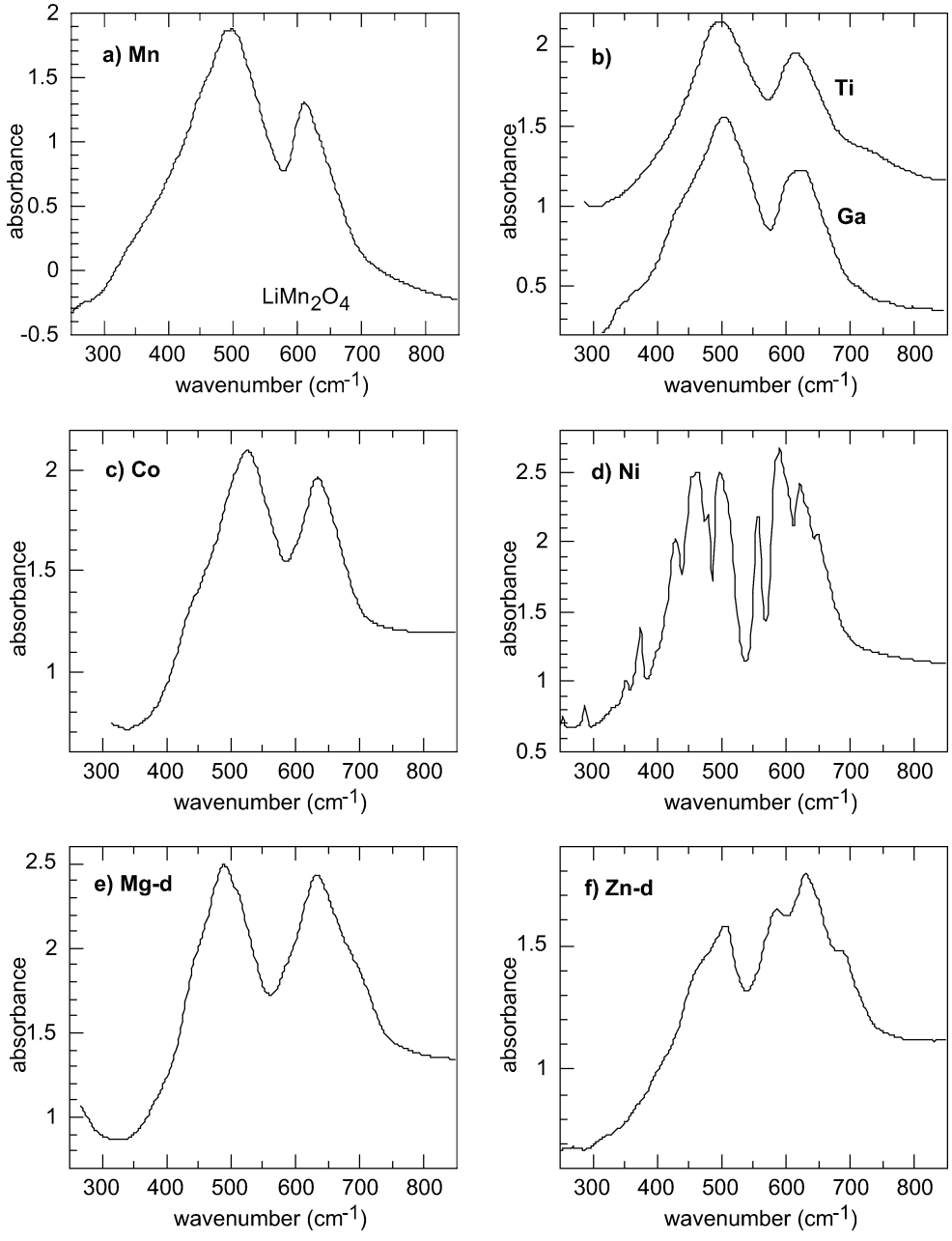

Fig. 4. FTIR spectra of selected substituted $LiMn_{1.5}M_{0.5}O_4$ (M indicated).

band frequencies between one group comprising trivalent substituents (Ga^{3+} and Co^{3+} (and Mn^{3+} as well), and a second group with divalent substituents Ni^{2+} and Zn^{2+}, which give higher frequencies of the T_{2g} and A_{1g} modes.

4. Discussion—structural trends

Table 2 shows that this work made available a wide range of manganese oxide spinels with cell parameter ranging from 8.138 to 8.304 Å, corresponding to substituents M with ionic radii from 0.525 (low-spin Co^{3+}) to 0.74 (Zn^{2+}) [42]. Bond distances and bond valence sums have been calculated (see Table 5). This allows to draw crystal chemical trends regarding the factor(s) determining (i) the cell dimensions, (ii) the occurrence of 1:3 16*d*-site cation ordering. Note that in calculating valence differences, Table 5 takes into account cation distribution inversion as evidenced from structural refinements: for instance the substituent on the octahedral site in the Zn-d sample is actually lithium, not zinc.

Focusing first on the cell parameter and 16*d* site–O distance, an examination of Table 5 shows that their values reflect the influence of two main factors: the substituent cationic radius r(M) and the manganese valence v(Mn). The fact that the cell parameter a decreases when a fraction of manganese is replaced by a larger cation such as Mg, Ni

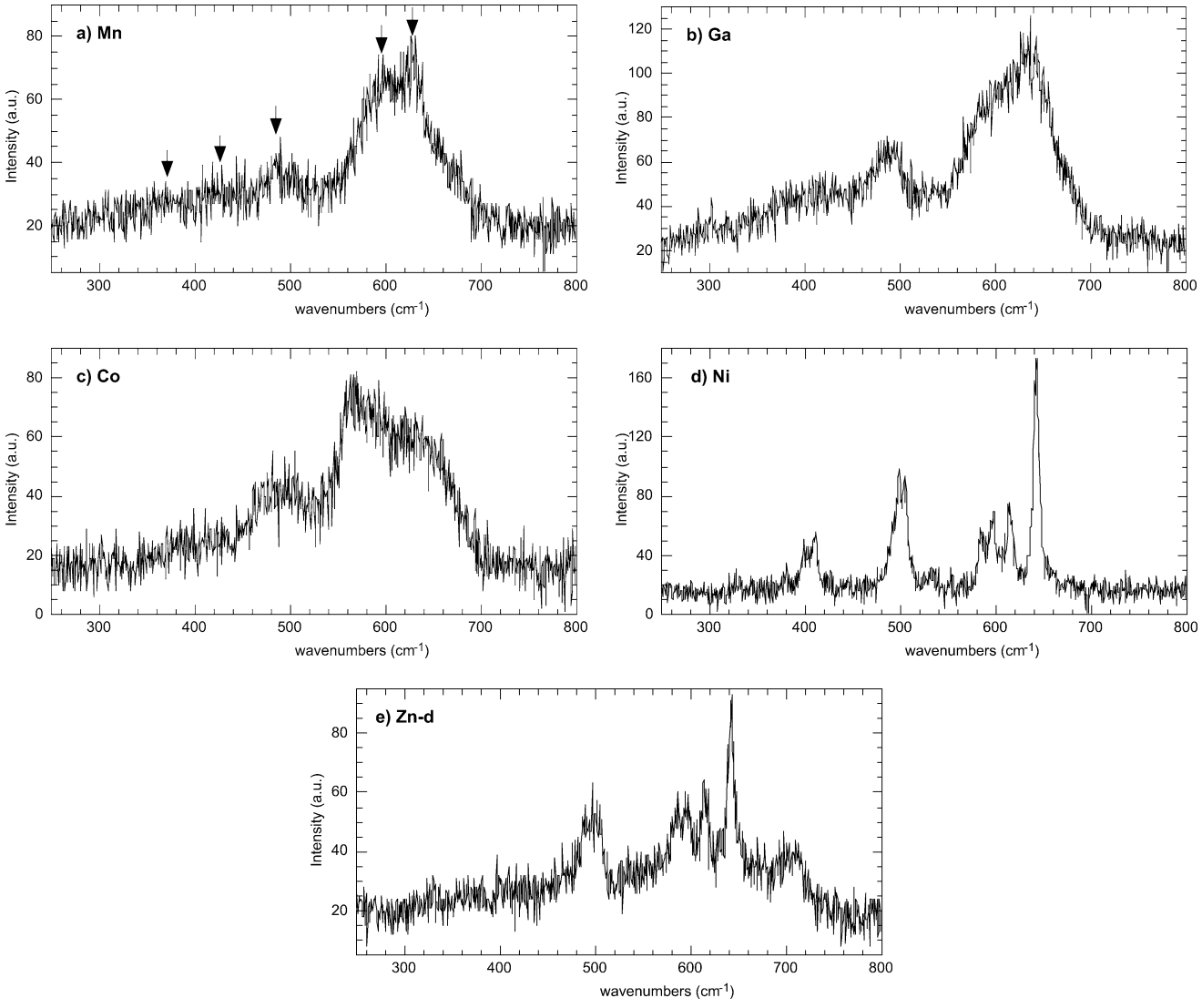

Fig. 5. Raman spectra of selected substituted $LiMn_{1.5}M_{0.5}O_4$ (M indicated). Arrows in panel (a) = positions of expected Raman-active modes.

Table 4
Observed Raman frequencies (in cm^{-1}) for $AMn_{1.5}M_{0.5}O_4$ samples

Mode	Intensity	Calc. [33]	Obs. [33]	Obs. [37]	Experimental results				
					Mn	Ga	Co	Ni	Zn-d
$T_{2g}(1)$	vw	354	365	370	368	366	380	411	405
E_g	w	434	432	435	421	424	(vw)		
$T_{2g}(2)$	m	455	480	482	486	488	481.5	498 + 505	496 (split?)
$T_{2g}(3)$	vs	597	590	580	588	593	572	triplet	triplet
A_{1g}	vs	598	625	625	627	639	635	642	642

or Cu shows that the dominant effect is that of manganese valence. However, the scattering in a values obtained for v(Mn) = 3.67 (see Table 5) shows that the manganese valence alone is not sufficient to determine a and d(16d–O). In fact, the best correlation is obtained using the average ionic radius on the 16d site $r_{\langle 16d \rangle}$, as shown in Fig. 6. This could be expected, since $r_{\langle 16d \rangle}$ includes the contributions of r(M) (for 25%) and of r(Mn), which in turn depends on v(Mn). This correlation confirms a previous report including M = Al, Co and Ti only [43]. The highest deviations are observed for the Zn samples, which have a more complex cation distribution.

This figure also confirms the charge distribution in the cobalt case: low-spin Co^{3+} is the smallest cation in this series and gives the lowest a and d(16d–O) values. Much higher cell parameter and Mn/Co–O distance would have

Table 5
Ionic radii r [40], cell parameter a, interatomic distances and BVS valences v in $AMn_{1.5}M_{0.5}O_4$ spinels AB_2O_4 [in increasing order of r(M)]. ⟨ ⟩ = average values

A	M	r(A) (Å)	r(M) (Å)	⟨r_{16d}⟩	v(M)	v(Mn)	Δ v Mn–M	Mn/M order	a (Å)	d(16d–O) (Å)	d(Mn–O) (Å)[b]	d(M–O) (Å)[b]	d(A–O) (Å)	v(Li) BVS	v(Mn) BVS	v(M(oct.)) BVS
Li	(Mn)[a]	”	–	0.585	–	3.5	0	–	8.246	1.958(1)			1.974(1)	1.07(4)	3.49(27)	
Li	Co	”	0.525	0.556	3	3.67	0.67	–	8.138	1.935(2)			1.944(2)	1.16(9)	_[d]	_[d]
Li	Ti	”	0.605	0.604	4	3.33	–0.67	–	8.304	1.974(2)			1.984(2)	1.04(2)	3.35(25)	3.93(5)
Li	Ga	”	0.62	0.58	3	3.67	0.67	–	8.211	1.954(2)			1.960(2)	1.10(6)	3.58(29)	3.32(19)[e]
$Li_{0.5}Mg_{0.5}$	Mg	⟨0.63⟩	0.67	0.59	2	3.67	1.67	–	8.279	1.973(1)			1.969(1)	Li 1.07(5) Mg 1.99(1)	3.38(27)	2.80(60)[e]
Li	Mg	”	0.67	0.565	2	4	2	+	8.187	⟨1.950⟩	⟨1.913⟩	2.062	⟨1.961⟩	1.14(8)	3.84(8)	2.27(15)
Li	Ni	0.59	0.69	0.57	2	4	2	+	8.167	⟨1.945⟩	1.911	2.051	⟨1.941⟩	1.13(8)	3.96(4)	2.08(4)
Li	Cu	”	0.73	0.58	2	4	2	+	8.189	⟨1.949⟩	1.921	2.034	⟨1.925⟩	1.09(5)	3.85(8)	2.32(19)
$Zn_{1-x}Li_x$	Zn/Li[c]	0.60	0.74	0.612	2	3.67	2.33	–	8.267	1.979(4)			1.949(4)	Li 1.14(6) Zn 2.17(10)	3.34(2)	Li 1.51(39)[e] Zn 2.87(63)
$Li_{0.5}Zn_{0.5}$	Li[c]	0.595	0.76	0.585	2	4	3	+	8.182	⟨1.952⟩	⟨1.906⟩	⟨2.091⟩ (Li)	Li ⟨1.903⟩ Zn ⟨2.016⟩	Li 1.14(8) Zn 1.85(7)	4.03(2)	Li 1.27(17)

[a] Reference unsubstituted compound.
[b] For ordered compounds → specific sites for Mn (12d) and M (4b).
[c] Significant Li/M inversion—see Table 2.
[d] Unapplicable (low-spin Co not taken into account by VaList program).
[e] Strained structure.

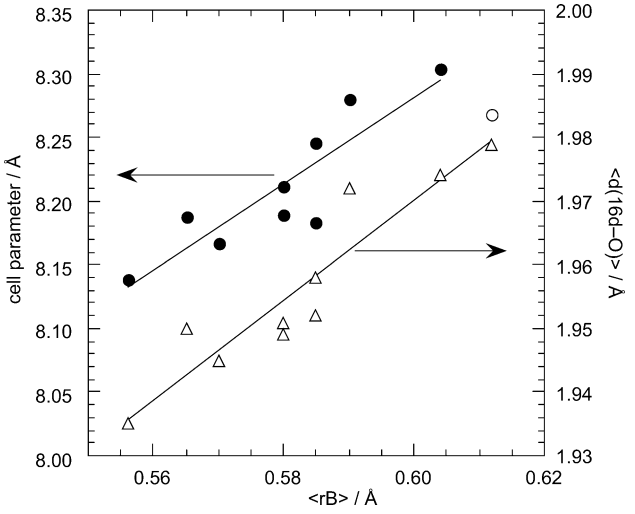

Fig. 6. Variation of cell parameter a and average octahedral site–oxygen distance d(16d–O) with average ionic radius of octahedral cation in the $LiMn_{1.5}M_{0.5}O_4$ series.

been expected for a Co^{2+}–Mn^{4+} distribution, since Co^{2+}, expected in high-spin configuration, has an octahedral ionic radius (0.74 Å) as large as those of Cu^{2+} or Zn^{2+} [42].

Turning now the occurrence of cation ordering, Table 5 shows that this effect seems to be related to the presence of large ionic radius substituents, which also correspond to the largest valence difference $\Delta v(Mn–M) \geqslant 2$. However, neither Mg-d nor Zn-d obey this trend, in spite of the large size of the substituent. These doubly-substituted samples differ from their $LiMn_{1.5}M_{0.5}O_4$ counterparts mostly by a lower manganese valence (+3.67 instead of +4). This results in (i) a lower valence difference Δv(Mn–M), (ii) a lower size difference, since a lower v(Mn) induces an increase in Mn–O bond length. We can thus conclude that cation ordering in this series requires (i) a large size difference, (ii) tetravalent manganese.

The separation of Mn and larger M atoms in distinct sites in space group $P4_332$ (or $P2_13$) allows to place the larger M atoms in bigger 4b sites (with M–O distances in the range 2.03–2.09 Å, and at the same time to reduce the cell volume: Table 5 shows that all cation-ordered phases have cell parameters smaller than the $Fd3m$ ones (with the exception of the cobalt phase), in spite of the presence of larger substituents. The net result is thus a significant optimization of space occupation. The largest size and valence difference is observed in the Zn sample, where the octahedral site substituent is actually lithium: this compound follows the trend outlined here, and yields the largest difference between the Mn–O and M–O distances (see Table 5, last line).

Finally, bond valence sum (BVS) have been calculated for all phases (see Table 5, last three columns). This factor is relevant for detecting implausible structures or strains on given atomic sites [44]. Among the unordered phases, the calculated BVS values exhibit significant valence shifts starting from the gallium case, indicating strains in the structure. This applies especially to the Mg-d and Zn-d phases,

where the large calculated v(BVS) for Mg and Zn indicate that these cations are under considerable compressive strain in their crystallographic site. As a consequence, the BVS calculation also gives too small manganese v(BVS). The splitting of octahedral sites among 12*d* and 4*b* sites in the $P4_332$ (or $P2_13$) space group allows to considerably relax these strains, as shown by the values for the Mg and Zn samples. The BVS values are in excellent agreement with expected valences in the nickel case. For Cu2, the agreement is only fair, probably due to the partial Li/Cu inversion and local Jahn–Teller distortion of the Cu^{2+} ion.

5. Conclusions

The present study addresses the question of cation ordering in Li–Mn–O spinels with 1/4 substitution on the octahedral sites. To overcome the inability of XRD to detect such ordering when the cations involved have undistinguishable scattering powers, neutron diffraction was used. This unambiguously showed the occurrence of octahedra site ordering for Ni and Cu substitution, while trivalent substituents (Ga, Co) or compositions with unsufficient charge difference between Mn and the substituting atom do not give rise to octahedral cation ordering. These results are confirmed by vibration spectroscopy (infrared and Raman), which clearly shows symmetry lowering in substituted spinels as a function of substituent.

6. Note added in proof

At the time of submitting this manuscript, we became aware of another structural study of the Li–Mn–Ni–O system [45]. Their results from neutron diffraction and FTIR spectroscopy for composition $Mn_{1.5}Ni_{0.5}O_4$ fully agree with the data presented here, (including also the presence of NiO impurity in the sample obtained).

Acknowledgements

The authors would like to thank Drs. E. Suard and O. Isnard for their assistance during neutron diffraction measurements at Institut Laue-Langevin, Grenoble.

References

[1] M.M. Thackeray, J. Ceram. Soc. Amer. 82 (1999) 3347.
[2] M. Broussely, P. Biensan, B. Simon, Electrochim. Acta 45 (1999) 3.
[3] G.G. Amatucci, A. Du Pasquier, A. Blyr, T. Zheng, J.M. Tarascon, Electrochim. Acta 45 (1999) 255.
[4] J.M. Tarascon, E. Wang, F.K. Shokoohi, W.R. McKinnon, S. Colson, J. Electrochem. Soc. 138 (1991) 2859.
[5] G.H. Li, H. Ikuta, T. Uchida, M. Wakihara, J. Electrochem. Soc. 143 (1996) 178.
[6] L. Hernan, J. Morales, L. Sanchez, E.R. Castellon, M.A.G. Aranda, J. Mater. Chem. 12 (2002) 734.
[7] H. Kawai, M. Nagata, H. Tukamoto, A.R. West, J. Power Sources 81–82 (1999) 67.
[8] G. Blasse, Philips Res. Rept. (1964) 1, JCPDS card 32-573.
[9] J.C. Joubert, A. Durif, C. R. Acad. Sci. Paris 258 (1964) 4482, JCPDS card 74-1260.
[10] Y.J. Lee, S.H. Park, C. Eng, J.B. Parise, C.P. Grey, Chem. Mater. 14 (2002) 194.
[11] J.S. Braithwaite, C.R.A. Catlow, J.H. Harding, J.D. Gale, Phys. Chem. Chem. Phys. 2 (2000) 38.
[12] S.M. Woodley, C.R.A. Catlow, P. Piszora, K. Stempin, E. Wolska, J. Solid State Chem. 153 (2000) 310.
[13] D. Gryffroy, R.E. Vandenberghe, E. Legrand, Mater. Sci. Forum 79 (1991) 785, ICSD # 70045 and 70046.
[14] P. Lagrange, D. Guérard, A. Hérold, J. Phys. Chem. Solids 53 (1992) 777, ICSD # 70023.
[15] W. Branford, M.A. Green, D.A. Neumann, Chem. Mater. 14 (2002) 1649.
[16] J. Preudhomme, Ann. Chim. (Paris) 9 (1974) 31.
[17] Y.J. Lee, C. Eng, C.P. Grey, J. Electrochem. Soc. 148 (2001) A249.
[18] F. Le Cras, D. Bloch, M. Anne, P. Strobel, Solid State Ionics 89 (1996) 203.
[19] P. Strobel, A. Ibarra-Palos, F. Le Cras, M. Anne, J. Mater. Chem. 10 (2000) 429.
[20] Rodriguez-Carvajal, Physica B 192 (1993) 55, www-llb.cea.fr/fullweb/powder.htm.
[21] A.S. Wills, Dept. of Chemistry, University College, London, UK; e-mail: a.s.wills@ucl.ac.uk.
[22] O. Muller, R. Roy, The Major Ternary Structural Families, Springer, Berlin, 1974, pp. 252–254.
[23] E. Rios, J.L. Gautier, G. Poillerat, P. Chartier, Electrochim. Acta 44 (1998) 1491.
[24] A.R. West, H. Kawai, H. Kageyama, M. Tabuchi, M. Nagata, H. Tukamoto, J. Mater. Chem. 11 (2001) 1662.
[25] P. Aitchison, B. Ammundsen, D.J. Jones, G. Burns, J. Roziere, J. Mater. Chem. 9 (1999) 3125.
[26] H.S.C. O'Neill, A. Navrotsky, American Mineralogist 68 (1983) 181, American Mineralogist 69 (1984) 733.
[27] A.N. Cormack, G.V. Lewis, S.C. Parker, C.R.A. Catlow, J. Phys. Chem. Solids 49 (1988) 53.
[28] V.F. Sears, AECL Report 8490 (1984).
[29] B. Gillot, S. Buguet, E. Kester, J. Mater. Chem. 7 (1997) 2513.
[30] W.B. White, B.A. De Angelis, Spectrochim. Acta 23A (1967) 985.
[31] T.J. Richardson, S.J. Wen, K.A. Striebel, P.N. Ross, E.J. Cairns, Mater. Res. Bull. 32 (1997) 609.
[32] C. Julien, M. Massot, E. Poniatowski, G.A. Nazri, A. Rougier, MRS Proc. 496 (1998) 415.
[33] B. Ammundsen, G.R. Burns, M.S. Islam, H. Kanoh, J. Rozière, J. Phys. Chem. B 103 (1999) 5175.
[34] G.C. Allen, M. Paul, Appl. Spectrosc. 49 (1995) 451.
[35] V.A.M. Brabers, Phys. Stat. Sol. A 12 (1972) 629.
[36] M. Laarj, S. Kacim, B. Gillot, J. Solid State Chem. 125 (1996) 67.
[37] S.R.S. Prabahanran, N.B. Saparil, S.S. Michael, M. Massot, C. Julien, Solid State Ionics 112 (1998) 25.
[38] C. Julien, S. Ziolkiewicz, M. Lemal, M. Massot, J. Mater. Chem. 11 (2001) 1837.
[39] C. Wu, Z. Wang, F. Wu, L. Chen, X. Huang, Solid State Ionics 144 (2001) 285.
[40] K. Dokko, M. Mohamedi, N. Anzue, T. Itoh, I. Uchida, J. Mater. Chem. 12 (2002) 3688.
[41] G.T.K. Fey, D.L. Huang, Electrochim. Acta 45 (1999) 295.
[42] R.D. Shannon, Acta Crystallogr. 32 (1976) 751.
[43] Y. Shao-Horn, R.L. Middaugh, Solid State Ionics 139 (2001) 13.
[44] I.D. Brown, Acta Crystallogr. B 48 (1995) 553.
[45] F.G.B. Ooms, E.M. Kelder, J. Schoonman, M. Wagemaker, F.M. Mulder, Solid State Ionics 152–153 (2002) 143.